Structural Engineering and Mechanics, Vol. 12, No. 6 (2001) 633-656
DOI: http://dx.doi.org/10.12989/sem.2001.12.6.633

Seismic test of modal control with direct output feedback for building structures

Lyan-Ywan Lu†

Department of Construction Engineering, National Kaohsiung First University of Science and Technology, 1 University Road, Yenchao, Kaohsiung 824, Taiwan

Abstract. In this paper, modal control with direct output feedback is formulated in a systematic manner for easy implementation. Its application to the seismic protection of structural systems is verified by a shaking table test, which involves a full-scale building model and an active bracing system as the control device. Two modal control cases, namely, one full-state feedback and one direct output feedback control were tested and compared. The experimental result shows that in mitigating the seismic response of building structures, modal control with direct output feedback can be as effective and efficient as that with full-state feedback control. For practical concerns, the control performance of the proposed method in the presence of sensor noise and stiffness modeling error was also investigated. The numerical result shows that although the control force may be increased, the maximum floor displacements of the controlled structure are very insensitive to sensor noise and modeling error.

Key words: active structural control; modal control; direct output feedback; seismic protection; active bracing system; shaking table test.

1. Introduction

It has been shown that the technique of active structural control can be an effective means for improving the serviceability and safety of civil engineering structures subjected to dynamic loading, such as wind or earthquake loads (Soong 1990, Nishitani 1998, Kurata *et al.* 1999, Lu *et al.* 1999). When compared with other engineering systems, a civil engineering structure usually has the following features: the mass and stiffness of the system are much larger; the time of life cycle is longer; the degrees of freedom for completely describing the system are larger. Therefore, a suitable active structural control system for a civil engineering structure must be able to deal with the above practical problems.

Generally speaking, an active structural control system is composed of mechanical actuators, response measurement sensors and a controller with a preloaded control algorithm that will decide how the actuator should react to external excitations. Among many control algorithms, modal control represents one control class, in which the motion of a structure is reshaped by merely controlling some selected vibration modes. In modern control theory, modal control is also called eigenvalue or pole assignment control. Modal control is especially desirable for the vibration control of civil engineering structures. The reason is that although a civil engineering structure, which is

† Associate Professor

usually a large structural system, may involve hundred or even thousand degrees of freedom, its vibration is usually dominated by the first few modes. Therefore, the motion of the structure can be effectively suppressed by merely controlling these few modes.

To date, numerous procedures and algorithms concerning modal control or pole assignment have been proposed in the literature. The works by Wonham (1967) and Simon and Mitter (1968) were among the first to analytically extend pole allocation problem from the classical single-input to a multiple-input control. In these early works, the number of inputs decided the complexity and details of each method. Later, the problem of eigenvalue assignment was reformulated and presented in different forms by Moore (1976), Porter and D'Azzo (1978) and Chang and Soong (1980). Although these precursory authors have paved a rigorous background for the modal control theory, their works primarily dealt with control using full state feedback.

A control method using full state feedback may not be practical for a structural system involving a large number of DOFs, since the control implementation may requires a large amount of sensors or a state observer of a huge dimension. In contrast, an output feedback control method, which requires the feedback of only some selected state variables of the controlled system, is more desirable. The papers by Davison (1970), Davison and Wang (1975), Kimura (1975), Srinathkumar (1978) represent some of the early works on modal control using direct output feedback (or incomplete state feedback). In these works, the procedures of computing the feedback gain were given and the limitations on eigenvalue assignability of the closed-loop system were also investigated extensively. More recently, Kautsky (1985) and Baruh (1987) proposed methods involving iterative minimization and recursive perturbation algorithms to accomplish pole placement using direct output feedback. Varga (1981) and Maghami and Juang (1989) proposed control methods utilized Schur matrix decomposition and coordinate transformation to alter one eigenvalue at a time recursively to the desired value. Balas (1979) and Lu *et al.* (1993) presented modal control methods that compute the feedback gain in a truncated modal space. Using a control method called independent modal space control (IMSC), Öz and Meirovitch (1980) and Chang and Yu (1998) showed that for a multiple DOF system, the modal property for each mode can be altered independently of the other modes.

The purpose of this study is to develop and experimentally verify a method of modal control with direct output feedback that is easily designed and implemented for active vibration control of seismic structures. The advantages of the control method proposed in the present paper includes that: First, the computation of the feedback gain is given in a systematic and concise matrix form, so that there is neither matrix decomposition nor recursive operation required. Second, the procedure for computing the best achievable eigenvectors that minimize the difference between the desired and achievable ones is also proposed, so that the designer has more freedom to select the desired mode shapes. The paper is organized as followings. The theoretical background of modal control as a tool of reshaping structural response is first reviewed and followed by the derivation of a matrix formula for computing the feedback gain. The constraints on the selection of eigenvalues and eigenvectors corresponding to the controllable modes are derived. To relax the constraints, the method for computing the best achievable eigenvectors is proposed. The set-up and result of a shaking table test that verified the proposed control method are described in detail. Finally, for practical concerns the influence of sensor noise and modeling error on the control performance of the proposed method is investigated numerically.

2. Relation between modal and eigen properties of structures

When a seismic structure is modeled by a lumped-mass n-DOF system, its equation of motion can be expressed by

$$\boldsymbol{M}_s\ddot{\xi}(t)+\boldsymbol{C}_s\dot{\xi}(t)+\boldsymbol{K}_s\xi(t)=-\boldsymbol{M}_s\boldsymbol{l}\ddot{x}_g(t) \tag{1}$$

where $\boldsymbol{M}_s$, $\boldsymbol{C}_s$ and $\boldsymbol{K}_s$ represent the mass, damping and stiffness matrices, respectively; the vector ξ denotes the relative nodal displacements of the structure with respect to the ground; $\ddot{x}_g$ represents the ground acceleration; $\boldsymbol{l}$ denotes the loading distribution vector. Generally speaking, a linear dynamic system described by Eq. (1) can be exclusively characterized by the n sets of modal parameters, namely, modal frequencies, damping ratios and mode shapes. In this paper, these parameters are, respectively, denoted by ω_i, ζ_i and $\boldsymbol{n}_i$ (i = 1, 2, … n), with the subscript i indicating that the entities are associated with the i-th vibration mode. These parameters can be evaluated by solving the eigenvalue problem of the homogeneous part of Eq. (1).

In the structural control theory, the equation of dynamics in Eq. (1) is usually converted into a first-order state space equation, i.e.,

$$\dot{\boldsymbol{x}}(t) = \boldsymbol{A}\boldsymbol{x}(t)+\boldsymbol{f}\,\ddot{x}_g(t) \tag{2}$$

where $\boldsymbol{x}(t)$ denotes the time-dependent state vector; $\boldsymbol{A}$ represents the time-invariant square matrix; $\boldsymbol{f}$ represents the seismic force distribution vector. These matrices can be shown explicitly as

$$\boldsymbol{x}(t) = \begin{Bmatrix}\dot{\xi}(t)\\ \xi(t)\end{Bmatrix} \in R^{2n\times 1} \quad \text{and} \quad \boldsymbol{f} = \begin{Bmatrix}-\boldsymbol{l}\\ 0\end{Bmatrix} \in R^{2n\times 1} \tag{3}$$

$$\boldsymbol{A} = \begin{bmatrix}-\boldsymbol{M}_s^{-1}\boldsymbol{C}_s & -\boldsymbol{M}_s^{-1}\boldsymbol{K}_s\\ \boldsymbol{I} & 0\end{bmatrix} \in R^{2n\times 2n} \tag{4}$$

where a symbol $R^{p\times q}$ indicates the dimension of a real-numbered matrix with p rows and q columns.

By inspecting Eq. (4) it is clear that the system matrix $\boldsymbol{A}$ preserves all the structural matrices $\boldsymbol{M}_s$, $\boldsymbol{C}_s$ and $\boldsymbol{K}_s$ of the original system; therefore, the eigen-properties of $\boldsymbol{A}$ should be related to the modal parameters of the system in Eq. (1). Since the matrices $\boldsymbol{M}_s$, $\boldsymbol{C}_s$ and $\boldsymbol{K}_s$ are all real, the matrix $\boldsymbol{A}$ is also real. For a real-numbered matrix, its eigenvalues and eigenvectors must be either real or appear as complex conjugate pairs. Let λ_{2i-1} and λ_{2i} be the i-th pair of the eigenvalues of $\boldsymbol{A}$, and $\boldsymbol{z}_{2i-1}$ and $\boldsymbol{z}_{2i}$ be the i-th pair of the eigenvectors. The relation between modal and eigen-parameters can be expressed by

$$\begin{aligned}\lambda_{2i-1} &= -\zeta_i\omega_i + j\,\omega_i\sqrt{1-\zeta_i^2}\\ \lambda_{2i} &= -\zeta_i\omega_i - j\,\omega_i\sqrt{1-\zeta_i^2}\end{aligned} \qquad \text{for } i = 1 \text{ to } n. \tag{5}$$

$$\boldsymbol{z}_{2i-1} = \begin{Bmatrix}\lambda_{2i-1}\boldsymbol{n}_i\\ \boldsymbol{n}_i\end{Bmatrix}, \quad \boldsymbol{z}_{2i} = \begin{Bmatrix}\lambda_{2i}\boldsymbol{n}_i\\ \boldsymbol{n}_i\end{Bmatrix} \qquad \text{for } i = 1 \text{ to } n. \tag{6}$$

Where $j = \sqrt{-1}$ and ζ_i, ω_i and $\boldsymbol{n}_i$ are the modal parameters defined previously. Eq. (5) and Eq. (6) give a one-to-one mapping between the modal parameters and the eigen-parameters for a given structure. In other words, if the modal parameters ω_i, ζ_i and $\boldsymbol{n}_i$ of a structure are specified, one can readily calculate their corresponding eigenvalues and eigenvectors by Eqs. (5) and (6). It is for this reason that modal control is also called eigenvalue assignment. On the other hand, given a pair of eigenvalues of $\boldsymbol{A}$, one may compute the corresponding modal frequency and damping ratio by solving Eq. (5), i.e.,

$$\begin{aligned} \omega_i &= \sqrt{\lambda_{2i-1}\lambda_{2i}} \\ \zeta_i &= \frac{-1}{2\omega_i}(\lambda_{2i-1} + \lambda_{2i}) \end{aligned} \tag{7}$$

From Eq. (7) it can be concluded that as long as the eigenvalues λ_{2i-1} and λ_{2i} are complex conjugate, ω_i and ζ_i are always two real numbers. Moreover, if ω_i is taken to be positive, the sign of ζ_i is always opposite to the sign of the real part of λ_{2i-1} and λ_{2i}. In other words, ζ_i (for i = 1, 2, … n) should be positive for a stable control system, since the real parts of all eigenvalues of a stable system should be negative.

3. Modal control with direct output feedback

3.1 Control closed-loop equation

When the seismic system denoted by Eq. (2) is equipped with active structural control devices, its equation of dynamics should be modified as

$$\dot{\boldsymbol{x}} = \boldsymbol{A}\boldsymbol{x} + \boldsymbol{B}\boldsymbol{u} + \boldsymbol{f}\,\ddot{x}_g \tag{8}$$

where the added term ($\boldsymbol{Bu}$) represents the effect of control forces, with $\boldsymbol{B}$ and $\boldsymbol{u}$ denoting the actuator placement matrix and the control force vector, respectively. Now, considering a control law of direct output feedback, where the control force vector $\boldsymbol{u}$ is determined by directly multiplying the sensor outputs by the feedback gain. The control closed-loop equation for this type of control laws may be written as

$$\begin{aligned} \dot{\boldsymbol{x}} &= (\boldsymbol{A} + \boldsymbol{BFC})\boldsymbol{x} + \boldsymbol{f}\,\ddot{x}_g \\ &= \boldsymbol{A}_c\boldsymbol{x} + \boldsymbol{f}\,\ddot{x}_g \end{aligned} \tag{9}$$

where $\boldsymbol{F}$ and $\boldsymbol{C}$ denote the feedback gain and the sensor placement matrix, respectively, while $\boldsymbol{A}_c$ represents the closed-loop system matrix. Let q and r be the numbers of sensors and actuators installed in the structure, respectively; therefore, the dimensions of the relevant matrices can be shown as $\boldsymbol{B} \in R^{2n\times r}$, $\boldsymbol{F} \in R^{r\times q}$, $\boldsymbol{C} \in R^{q\times 2n}$ and $\boldsymbol{A}_c \in R^{2n\times 2n}$. It should be noted that a closed-loop equation with the form given by Eq. (9) assumes the feedback signals being the structural velocities and/or displacements only. For the time being, the control with acceleration feedback (Dyke *et al.* 1996a and 1996b) is thus not considered here.

In view of Eq. (9), the meaning of modal control is to properly design the feedback gain matrix $\boldsymbol{F}$

so that the added term ($\boldsymbol{B}\ \boldsymbol{F}\ \boldsymbol{C}$) will alter the eigen-structure of the open-loop system matrix $\boldsymbol{A}$ to that of the matrix $\boldsymbol{A}_c$ in a desired or prescribed manner. In the next sub-section, a matrix equation for computing the feedback gain $\boldsymbol{F}$ is derived. The equation gives a systematic way of generating the gain matrix, once the target eigenvalues are given. The gain matrix allows the number of the controllable eigenvalues and eigenvectors be equal to the number of sensor measurements, q.

3.2 Design of feedback gain

Let λ_i and $\boldsymbol{u}_i$ denote the i-th eigenvalue and eigenvector of the closed-loop matrix $\boldsymbol{A}_c$. From Eq. (9), we have

$$\boldsymbol{A}_c\boldsymbol{u}_i = (\boldsymbol{A} + \boldsymbol{BFC})\boldsymbol{u}_i = \lambda_i\boldsymbol{u}_i \tag{10}$$

Next, let the matrices $\boldsymbol{A}$ and $\boldsymbol{B}$ be partitioned as

$$\boldsymbol{A} = \begin{bmatrix} \boldsymbol{A}_1 \\ \boldsymbol{A}_2 \end{bmatrix} \text{ and } \boldsymbol{B} = \begin{bmatrix} \boldsymbol{B}_1 \\ \boldsymbol{B}_2 \end{bmatrix} \tag{11}$$

where $\boldsymbol{A}_1 \in R^{r\times 2n}$ and $\boldsymbol{B}_1 \in R^{r\times r}$. Substituting $\boldsymbol{A}$ and $\boldsymbol{B}$ from Eq. (11) into Eq. (10) yields two separate matrix equations

$$(\boldsymbol{A}_1 + \boldsymbol{B}_1\boldsymbol{FC})\boldsymbol{u}_i = \lambda_i\boldsymbol{z}_i \tag{12}$$

$$(\boldsymbol{A}_2 + \boldsymbol{B}_2\boldsymbol{FC})\boldsymbol{u}_i = \lambda_i\boldsymbol{w}_i \tag{13}$$

where $\boldsymbol{z}_i \in R^{r\times 1}$ and $\boldsymbol{w}_i \in R^{(2n-r)\times 1}$ represent the upper and lower partitions of $\boldsymbol{u}_i$.

Now, let the number of eigenvalues and eigenvectors assigned by the control designer be q, and also let the target values of these eigenvalues and eigenvectors be denoted by $\lambda_i^{(c)}$ and $\boldsymbol{u}_i^{(c)}$, where i = 1, 2, ..., q (a superscript (c) indicates that the entity is associated with the control target modes). Substituting these assigned values and vectors into Eq. (12) one by one, one can collect the q equations to form an enlarged matrix equation, i.e.,

$$(\boldsymbol{A}_1 + \boldsymbol{B}_1\boldsymbol{FC})\boldsymbol{U}_c = \boldsymbol{Z}_c\mathrm{diag}(\lambda_i)_c \tag{14}$$

where

$$\boldsymbol{U}_c = [\boldsymbol{u}_1^{(c)}, \boldsymbol{u}_2^{(c)}, \ldots, \boldsymbol{u}_q^{(c)}] \tag{15}$$

and

$$\mathrm{diag}(\lambda_i)_c = \begin{bmatrix} \lambda_1^{(c)} & 0 & \cdots & 0 \\ 0 & \lambda_2^{(c)} & & \vdots \\ \vdots & & \ddots & 0 \\ 0 & \cdots & 0 & \lambda_q^{(c)} \end{bmatrix} \tag{16}$$

Also, in Eq. (14) $\boldsymbol{Z}_c$ is the upper partition of $\boldsymbol{U}_c$, i.e.,

$$\boldsymbol{U}_c = \begin{Bmatrix} \boldsymbol{Z}_c \\ \boldsymbol{W}_c \end{Bmatrix} \tag{17}$$

where the dimensions of the sub-matrices are $\boldsymbol{Z}_c \in R^{r\times q}$ and $\boldsymbol{W}_c \in R^{(2n-r)\times q}$. Finally, from Eq. (14) one can immediately solve for the gain matrix $\boldsymbol{F}$ and obtains

$$\boldsymbol{F} = \boldsymbol{B}_1^{-1}(\boldsymbol{Z}_c \mathrm{diag}(\lambda_i)_c - \boldsymbol{A}_1\boldsymbol{U}_c)(\boldsymbol{C}\boldsymbol{U}_c)^{-1} \tag{18}$$

By substituting $\boldsymbol{F}$ from Eq. (18) back to Eq. (10), one can prove that the closed-loop system matrix $\boldsymbol{A}_c$ will possess the desired eigenpairs $(\lambda_i^{(c)}, \boldsymbol{u}_i^{(c)})$ for i = 1, 2, ..., q. In Eq. (18), the gain $\boldsymbol{F}$ has a solution only if the square matrices $\boldsymbol{B}_1$ and $(\boldsymbol{C}\boldsymbol{U}_c)$ are both non-singular. In the cases that the matrices $\boldsymbol{B}_1$ or $(\boldsymbol{C}\boldsymbol{U}_c)$ happens to be singular, one may reorder the rows of the matrix $\boldsymbol{B}$ or redesign the eigenvectors $\boldsymbol{U}_c$ in order to avoid the matrix singularity.

In Eq. (18), it seems that the requirements on the system controllability and observability do not explicitly appear in the computation of the gain. However, it has been shown by Davison (1970) that for the direct output feedback control system described by Eq. (9), the system must be controllable and observable, then the gain matrix $\boldsymbol{F}$ is able to assign q eigenvalues (let $q > r$) of $\boldsymbol{A}_c$ arbitrarily close to q prescribed values. Furthermore, it should be noted that although the gain computed by Eq. (18) is able to assign $q/2$ structural modes to the prescribed modal parameters, mathematically it does not guarantee which modes will be changed. However, as it will be shown in the later sections that as long as the modal frequencies of the control target modes remain unchanged, the damping ratios and the mode shape elements of these target modes can be altered precisely to the prescribed values.

3.3 Derivation of achievable eigenvectors

In the previous discussion, it was shown how the q arbitrary eigenvalues and eigenvectors of the closed-loop matrix $\boldsymbol{A}_c$ can be altered to the desired values by the proposed formula. Recall that the constraint number q is the number of sensors installed in the structure. However, in this paper, it is further shown that not all of the elements in the corresponding q eigenvectors can be arbitrarily assigned but only r elements in each eigenvector can be freely selected. The derivation is presented below.

By substituting the pre-selected q target eigenpairs $\lambda_i^{(c)}$ and $\boldsymbol{u}_i^{(c)}$ (where i = 1, 2, ..., q) into Eq. (13) one by one and combining these q equations together, one may obtain a single enlarged matrix equation similar to Eq. (14), i.e.,

$$(\boldsymbol{A}_2 + \boldsymbol{B}_2\boldsymbol{F}\boldsymbol{C})\boldsymbol{U}_c = \boldsymbol{W}_c \mathrm{diag}(\lambda_i)_c \tag{19}$$

where $\boldsymbol{U}_c$ and $\boldsymbol{W}_c$ are defined in Eqs. (15) and (17). Now, substituting $\boldsymbol{F}$ from Eq. (18) into Eq. (19) leads to

$$(\boldsymbol{A}_2 - \boldsymbol{B}_2\boldsymbol{B}_1^{-1}\boldsymbol{A}_1)\boldsymbol{U}_c + \boldsymbol{B}_2\boldsymbol{B}_1^{-1}\boldsymbol{Z}_c \mathrm{diag}(\lambda_i)_c = \boldsymbol{W}_c \mathrm{diag}(\lambda_i)_c \tag{20}$$

Next, let us further partition the matrices $\boldsymbol{A}_1$ and $\boldsymbol{A}_2$ of Eq. (11) as

$$\boldsymbol{A} = \begin{bmatrix} \boldsymbol{A}_1 \\ \boldsymbol{A}_2 \end{bmatrix} = \begin{bmatrix} \boldsymbol{A}_{11} & \boldsymbol{A}_{12} \\ \boldsymbol{A}_{21} & \boldsymbol{A}_{22} \end{bmatrix} \tag{21}$$

where $\boldsymbol{A} \in R^{2n\times 2n}$, $\boldsymbol{A}_{11} \in R^{r\times r}$ and $\boldsymbol{A}_{21} \in R^{(2n-r)\times r}$. Using Eqs. (21), one can rewrite Eq. (20) as

$$\boldsymbol{W}_c \mathrm{diag}(\lambda_i)_c - \boldsymbol{S}_3\boldsymbol{W}_c = \boldsymbol{S}_2\boldsymbol{Z}_c + \boldsymbol{S}_1\boldsymbol{Z}_c \mathrm{diag}(\lambda_i)_c \tag{22}$$

where

$$\boldsymbol{S}_1 = \boldsymbol{B}_2\boldsymbol{B}_1^{-1},\ \boldsymbol{S}_2 = (\boldsymbol{A}_{21} - \boldsymbol{S}_1\boldsymbol{A}_{11}),\ \boldsymbol{S}_3 = (\boldsymbol{A}_{22} - \boldsymbol{S}_1\boldsymbol{A}_{12}) \tag{23}$$

Note that the three constant matrices $\boldsymbol{S}_1$, $\boldsymbol{S}_2$, and $\boldsymbol{S}_3$ merely depend on the sub-matrices of the system matrix $\boldsymbol{A}$ and the actuator location matrix $\boldsymbol{B}$.

Although Eq. (22) gives the relation between $\boldsymbol{W}_c$ and $\boldsymbol{Z}_c$, i.e., the lower and the upper portions of $\boldsymbol{U}_c$, one can not use the equation directly to express $\boldsymbol{W}_c$ in terms of $\boldsymbol{Z}_c$. To solve this problem, one may decompose Eq. (22) into q equations, so that each equation is related to one assigned eigenpair only, i.e.,

$$(\lambda_i^{(c)}\boldsymbol{I}_1 - \boldsymbol{S}_3)\ \boldsymbol{w}_i^{(c)} = (\boldsymbol{S}_2 + \lambda_i^{(c)}\boldsymbol{S}_3)\boldsymbol{z}_i^{(c)} \qquad (\text{for } i = 1, 2, ..., q) \tag{24}$$

where $\boldsymbol{z}_i$ and $\boldsymbol{w}_i$ are the i-th columns of $\boldsymbol{Z}_c$ and $\boldsymbol{W}_c$, respectively, and $\boldsymbol{I}_1$ is an identity matrix of the dimension $(2n–r)\times(2n–r)$. Provided that $(\lambda_i^{(c)}\boldsymbol{I}_1–\boldsymbol{S}_3)$ is not a singular matrix, one can solve Eq. (24) for $\boldsymbol{w}_i^{(c)}$ in terms of $\boldsymbol{z}_i^{(c)}$. Finally, using this solution in $\boldsymbol{u}_i^{(c)}$ yields

$$\boldsymbol{u}_i^{(c)} = \begin{Bmatrix} \boldsymbol{z}_i^{(c)} \\ \boldsymbol{w}_i^{(c)} \end{Bmatrix} = \boldsymbol{L}_i\boldsymbol{z}_i^{(c)} \tag{25}$$

where

$$\boldsymbol{L}_i = \begin{Bmatrix} \boldsymbol{I}_2 \\ (\lambda_i^{(c)}\boldsymbol{I}_1 - \boldsymbol{S}_3)^{-1}(\boldsymbol{S}_2 + \lambda_i^{(c)}\boldsymbol{S}_1) \end{Bmatrix} \tag{26}$$

and $\boldsymbol{I}_2$ is an identity matrix of the dimension $(r\times r)$. The vector $\boldsymbol{u}_i^{(c)}$ expressed by Eq. (25) is referred to as the achievable eigenvector (Andry *et al.* 1983). Two observations can be made from the last two equations: (1) $\boldsymbol{u}_i^{(c)}$ must lay in the subspace spanned by the columns in $\boldsymbol{L}_i$, so the number of free parameters can be assigned in $\boldsymbol{u}_i^{(c)}$ is equal to the number of elements in $\boldsymbol{z}_i^{(c)}$, which is r. (2) The coefficient matrix $\boldsymbol{L}_i$ depends on the target eigenvalue $\lambda_i^{(c)}$, the uncontrolled system matrix $\boldsymbol{A}$ and the actuator location matrix $\boldsymbol{B}$, but not the gain matrix $\boldsymbol{F}$.

3.4 Best achievable eigenvectors

As shown above, an achievable eigenvector can not be arbitrarily selected and it must obey the condition given by Eq. (25). This implies that once the free elements in vector $\boldsymbol{z}_i^{(c)}$ were selected, the rest of the elements in $\boldsymbol{u}_i^{(c)}$ are also decided immediately. In other words, the control designer may have the freedom to choose the values of the elements in $\boldsymbol{z}_i^{(c)}$ but he also completely loses the freedom to design the rest of the elements in $\boldsymbol{u}_i^{(c)}$. From the designer's point of view, this may not

be the desired situation. An alternative approach to decide the achievable eigenvectors is proposed below. This approach, which minimizes the difference between the desired and achievable vectors, allows the designer to alter more elements in each designed eigenvector.

First, let $\boldsymbol{u}_i^{(d)}$ and $\boldsymbol{u}_i^{(c)}$ be the i-th desired and achievable eigenvectors, respectively. Here, the desired vector $\boldsymbol{u}_i^{(d)}$ is the one that the designer will prescribe all the elements for as he thinks best for the structural system. Let us define an index J that is the square norm of the difference between the two vectors $\boldsymbol{u}_i^{(d)}$ and $\boldsymbol{u}_i^{(c)}$

$$J = \left\| \boldsymbol{u}_i^{(d)} - \boldsymbol{u}_i^{(c)} \right\|^2 = \left\| \boldsymbol{u}_i^{(d)} - \boldsymbol{L}_i \boldsymbol{z}_i^{(c)} \right\|^2 \tag{27}$$

Among all of possible vectors of $\boldsymbol{z}_i^{(c)}$, the one that minimizes the index J is defined as the best vector. After it is substituted into Eq. (25), this best vector will produce the best achievable eigenvector $\boldsymbol{u}_i^{(c)}$. To obtain the best vector $\boldsymbol{z}_i^{(c)}$, one may take the following two derivatives and set them equal to zero

$$\frac{\partial J}{\partial \boldsymbol{z}_{iR}^{(c)}} = \boldsymbol{0}, \quad \frac{\partial J}{\partial \boldsymbol{z}_{iI}^{(c)}} = \boldsymbol{0} \tag{28}$$

where $\boldsymbol{z}_{iR}^{(c)}$ and $\boldsymbol{z}_{iI}^{(c)}$ are the real and the imaginary parts of $\boldsymbol{z}_i^{(c)}$. Furthermore, using the expression of $\boldsymbol{u}_i^{(d)} = \boldsymbol{u}_{iR}^{(d)} + j\boldsymbol{u}_{iI}^{(d)}$ and $\boldsymbol{L}_i = \boldsymbol{L}_{iR} + j\boldsymbol{L}_{iI}$ in Eqs. (27) and (28) leads to the following simultaneous equations

$$\begin{bmatrix} \boldsymbol{L}_{iR}^T\boldsymbol{L}_{iR} + \boldsymbol{L}_{iI}^T\boldsymbol{L}_{iI} & \boldsymbol{L}_{iI}^T\boldsymbol{L}_{iR} - \boldsymbol{L}_{iR}^T\boldsymbol{L}_{iI} \\ \boldsymbol{L}_{iR}^T\boldsymbol{L}_{iI} - \boldsymbol{L}_{iI}^T\boldsymbol{L}_{iR} & \boldsymbol{L}_{iR}^T\boldsymbol{L}_{iR} + \boldsymbol{L}_{iI}^T\boldsymbol{L}_{iI} \end{bmatrix} \begin{Bmatrix} \boldsymbol{z}_{iR}^{(c)} \\ \boldsymbol{z}_{iI}^{(c)} \end{Bmatrix} = \begin{Bmatrix} \boldsymbol{L}_{iR}^T\boldsymbol{u}_{iR}^{(d)} + \boldsymbol{L}_{iI}^T\boldsymbol{u}_{iI}^{(d)} \\ \boldsymbol{L}_{iR}^T\boldsymbol{u}_{iI}^{(d)} - \boldsymbol{L}_{iI}^T\boldsymbol{u}_{iR}^{(d)} \end{Bmatrix} \tag{29}$$

Since $\boldsymbol{u}_{iR}^{(d)}$ and $\boldsymbol{u}_{iI}^{(d)}$ are given by the designer, the only unknowns in Eq. (29) are $\boldsymbol{z}_{iR}^{(c)}$ and $\boldsymbol{z}_{iI}^{(c)}$. Solving Eq. (29) and substituting the solutions of $\boldsymbol{z}_{iR}^{(c)}$ and $\boldsymbol{z}_{iI}^{(c)}$ into Eq. (25), one shall obtain the best achievable eigenvector $\boldsymbol{u}_i^{(c)}$.

4. Experimental verification by shaking table test

In order to verify the feasibility of the aforementioned modal control scheme, a shaking table test was conducted in the Earthquake Simulation Laboratory of the National Center for Research on Earthquake Engineering (NCREE), Taipei, Taiwan. A full-scale three-story building model was erected on the shaking table for the test. An active bracing system assembled in the laboratory was used as the active structural control device. The test facility, instrumentation, ground motion, etc. are described in this section.

4.1 Test facility and building model

The shaking table facility located in the laboratory of NCREE has a table size of 5×5 m and is able to simulate a three-directional ground motion. The maximum allowable payload for the table is 50 metric tons. The test model, which is a three-story steel frame, is assembled from grade A36 H-shape steel beams. Fig. 1 shows the dimensions of the steel model mounted on the shaking table.

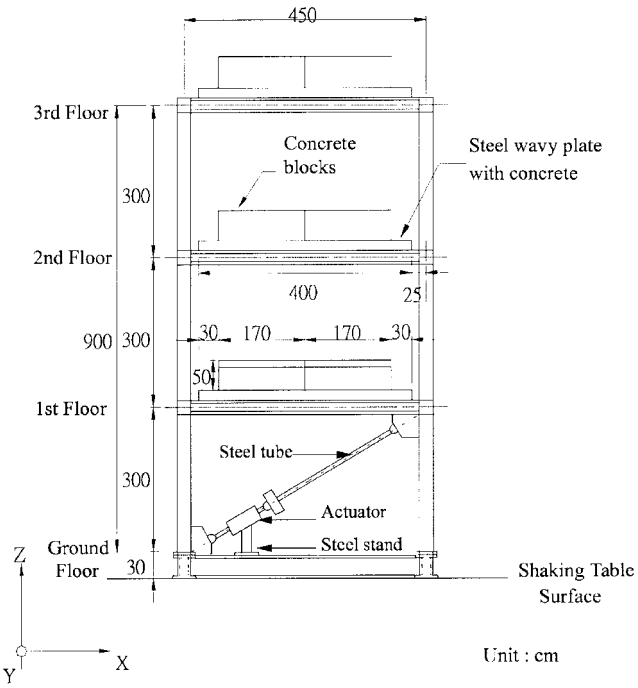

Fig. 1 Full-scale three-story steel building model with active bracing system

Note that in the figure the first floor denotes the floor above the ground floor. All the columns of the steel frame are made of H200 × 200 × 8 × 12 (mm) steel, while the girders are of H200 × 150 × 6 × 9 (mm) steel. The model has a uniform story height of 3 m, so the elevation of the roof is 9 m. The top-view plane dimension of the frame is 3 by 4.5 m (width and depth). Several concrete blocks are fixed on each floor to simulate the floor mass. The total mass of the structure model is about 30 metric tons. In order to obtain the actual modal parameters of the building model, a modal identification test was conducted prior to the formal test. In that test, a wide-band white-noise excitation was imposed on the model by the shaking table; afterward, a modal analysis using the test data was carried out. The modal parameters identified from the test are shown in the second column of Table 1. These modal values were required for the design of the feedback gain $\boldsymbol{F}$. Furthermore, based on the identified modal parameters, Table 2 lists the synthesized structural matrices that were employed in the computation of the analytical control results.

4.2 Active bracing system and its proof test

A laboratory-made active bracing system was built for this study, in order to provide the control forces for the test model. The system included a pair of active braces that were placed in parallel on the two sides of the first story panel (i.e., between the ground and first floors, see Fig. 1) and installed as diagonal members. Each active brace was built by connecting an electric-hydraulic actuator to a steel tube (see Fig. 2). The specifications of the components of the active braces are listed in Table 3. The active braces were rigidly connected to the frame. Each brace was properly aligned so that the centerline of each brace passed through the centers of the beam-column

Table 1 Modal properties of steel frame with various control conditions

Modal parameters	Control case					
	Uncontrolled (bare frame)		Case DV123		Case DV1	
Modal frequency[(1)] (Hz)		1.07		**1.07**		**1.07**
		3.48		**3.48**		3.52
		5.98		**5.98**		5.66
Damping ratios[(1)] (%)		1.41		**15.00**		**15.00**
		0.44		**15.00**		30.43
		0.31		**15.00**		9.51
1st mode shape[(2) (3)]	2.76	(0.00°)	2.56	(15.59°)	2.56	(15.59°)
	2.19	(0.00°)	2.05	(11.58°)	2.05	(11.58°)
	1.00	(0.00°)	1.00	(0.00°)	1.00	(0.00°)
2nd mode shape[(2) (3)]	0.80	(180.00°)	0.74	(178.03°)	0.57	(172.32°)
	0.53	(0.00°)	0.53	(26.21°)	0.54	(43.22°)
	1.00	(0.00°)	1.00	(0.00°)	1.00	(0.00°)
3rd mode shape[(2) (3)]	0.53	(0.00°)	0.39	(60.19°)	0.69	(52.90°)
	1.11	(180.00°)	0.82	(−30.73°)	1.34	(−34.57°)
	1.00	(0.00°)	1.00	(0.00°)	1.00	(0.00°)
Remark	Parameters identified from a modal test		Full state feedback control, 6 sensors used		Direct output feedback control, 2 sensors used	

[(1)] Data listed from the 1st to the 3rd modes.
[(2)] The degrees of freedom are labeled from the 3rd to the 1st floors.
[(3)] Complex vector expressed by its magnitude and phase angle (in parenthesis).

Table 2 Structural matrices used for numerical analysis

Mass	$\boldsymbol{M} = \begin{bmatrix} 10.914 & 0 & 0 \\ 0 & 11.213 & 0 \\ 0 & 0 & 11.213 \end{bmatrix}$	ton
Damping	$\boldsymbol{C} = \begin{bmatrix} 2.124 & -1.131 & 0.093 \\ -1.131 & 2.364 & -0.209 \\ 0.093 & -0.209 & 2.325 \end{bmatrix}$	kN/(m/s)
Stiffness	$\boldsymbol{K} = \begin{bmatrix} 3673.845 & -4555.417 & 1172.960 \\ -4556.112 & 8753.602 & -5451.810 \\ 1172.190 & -5452.178 & 9186.159 \end{bmatrix}$	kN/m

connections of the frame.

In addition to the active braces, the complete active bracing system also included an analog controller, a digital-to-analog converter, a personal computer and a mobile hydraulic power supplier (see Fig. 3). The computer, which performed as the central processing unit of control, did the following on-line tasks: receiving the sensor measurements $\boldsymbol{y}$, computing the required control forces $\boldsymbol{u}$ ($\boldsymbol{u} = \boldsymbol{F}\,\boldsymbol{y}$) and sending the commands to the actuators.

In order to assure test safety and also reduce experimental uncertainty, a proof test was performed on the active bracing system alone before the system was installed on the building model. The purpose of the test was to investigate the consistency between the control command and the actual

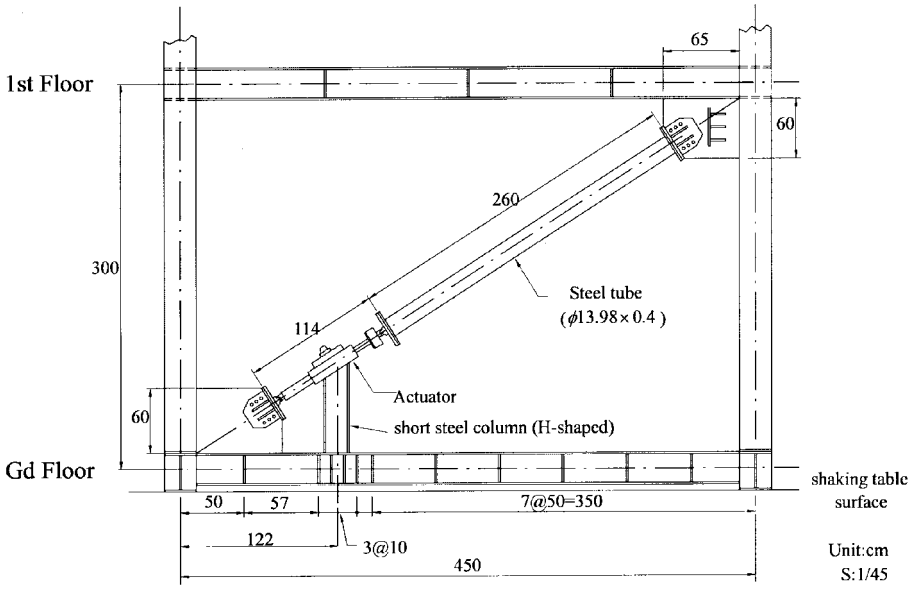

Fig. 2 Installation of active bracing system in the first floor panel

Table 3 Specifications of active bracing system

Component	Property	Specification
Steel tube	Diameter	13.98 cm
	Thickness	0.4 cm
	Length	260 cm
	Young's Modulus	2.04×10^6 kgf/cm^2
	Stiffness	133934 kgf/cm
Actuator	Force capacity	2.55 ton
	Max. stroke	± 7.5 cm
	Rod diameter	4.45 cm
	Piston area	135 cm^2
Hydraulic system	Max. Flow rate	10 gpm
	Working pressure	3000 psi

control force provided by the active brace. The actual control force was measured by the load cell embedded in the actuator. In the test, the two ends of a single active brace were rigidly fixed between a reaction wall and a reaction frame. By doing so, the dynamic effect of the structure was excluded from the test.

To show the result of proof test, let $u(t)$ be the control command and $u'(t)$ be the measured control force at any given time (see Fig. 3) and also let their ratio in the frequency domain be $H(\omega) = U'(\omega)/U(\omega)$. The Fourier function $H(\omega)$, which is a complex function, is equivalent to the output-to-input transfer function of the active bracing system. Let $|H(\omega)|$ and $\phi(\omega)$ represent, respectively, the amplitude and phase angle of the transfer function. Physically, $|H(\omega)|$ and $\phi(\omega)$

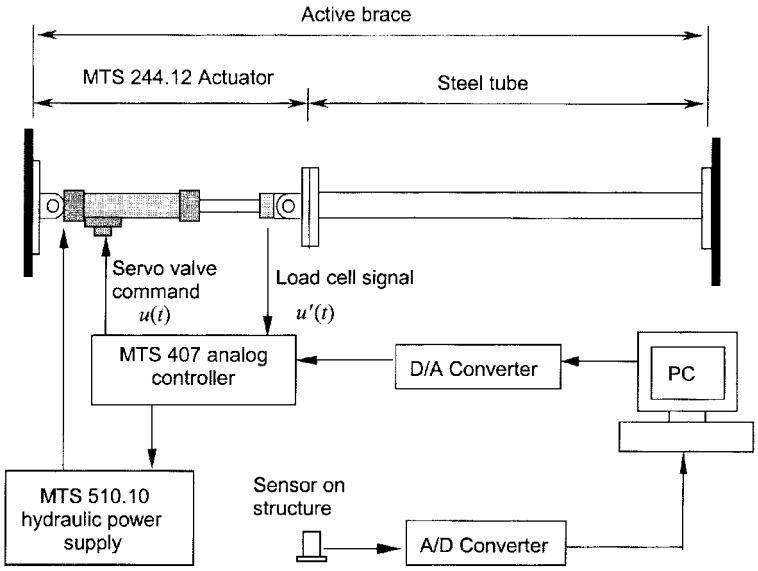

Fig. 3 Schematic diagram of active bracing system

are directly related to the magnification factor and the time-lag of the active bracing system. For an ideal control system, where the output force follows exactly the input command, the values of the amplitude and phase should be $|H(\omega)| = 1$ and $\phi(\omega) = 0$ within the operating frequency range. Figs. 4(a) and (b) depict the experimental values of $|H(\omega)|$ and $\phi(\omega)$ for the active bracing system.

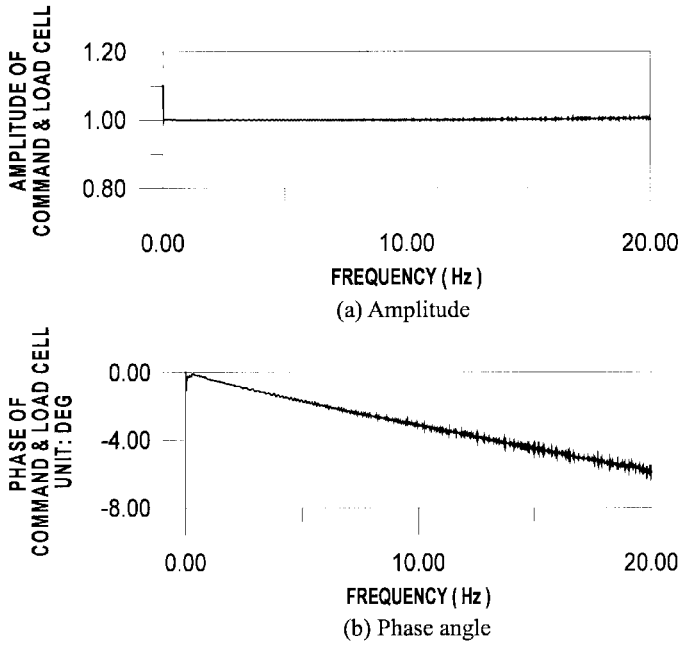

(a) Amplitude

(b) Phase angle

Fig. 4 Output/input transfer function of active bracing system

It is shown by the figures that the amplitude is very close to unity and the phase lag is only about 6 degrees even at a high frequency of 20 Hz, which represents a mere 0.0008333 second of control time delay.

4.3 Input ground motion and instrumentation

In the experiment, only the horizontal components of El Centro (1940) and Kobe (1995) earthquake records with PGA scaled down to 0.1g were used as the input ground motion. A displacement transducer (manufactured by Temposonics Co., type II) and a velocity sensor (by Tokyo Sokushin Co., model VSE-15) were mounted on each floor and also on the shaking table, so that the relative response of the test model to the ground can be measured. The signals of some transducers and sensors mentioned above were also used for feedback control when they were needed. The steel model was assumed to be a two-dimensional shear building, so only its horizontal motion along the long axis was recorded.

5. Test results and discussions

5.1 Control cases tested

Two control cases with different sensor feedback were conducted in the shaking table test. In the first case (labeled DV123 in the following figures), six sensor signals representing the full-state of the model were fed back to the controller. The full-state signals include the relative displacements and velocities of all three floors (the term “relative” means the response is measured relative to the ground). In the second case (labeled DV1), only the partial state information, namely, the relative displacement and velocity of the first floor were fed back to the controller, so only two sensors were needed. The second case represents the direct output feedback control.

From the previous discussion, it is known that for the proposed modal control, the number of the controllable eigenvalues is equal to the number of sensors available and two eigenvalues physically represent one vibration mode. Therefore, in the first case (where $q = 6$) all three vibration modes were controllable, while in the second case (where $q = 2$), only one vibration mode could be controlled. The first mode was chosen as the control target mode in the second case, since it dominates the vibration of the model.

The control goal for both cases was chosen such that the damping ratios of the control target modes were increased to 15% while at the same time their corresponding modal frequencies and desired mode shapes remained unchanged. The desired eigenvalues and eigenvectors complied with the above control goal were first computed by using Eqs. (5) and (6). Then, the best achievable eigenvectors, which are closest to the desired ones, were computed by Eqs. (25) and (29). Finally the desired eigenvalues and the best achievable eigenvectors were substituted into Eq. (18) for the computation of the feedback gain $\boldsymbol{F}$.

5.2 Frequency domain data

The last two columns of Table 1 show the equivalent modal values resulted from the two control cases. These values are independent of input ground motions. Also shown in the table are the modal

values of the uncontrolled structure (before the active bracing system was installed). As can be seen in the table, the steel model itself had very small inherent damping ratios. Furthermore, Table 1 also shows that: (1) In control case DV123 (full-state feedback), the damping ratios of all three modes have reached the target values 15%, and also all the frequencies remained unchanged. (2) In control case DV1 (direct output feedback) only the first mode (control target mode) has achieved the control goal, i.e., 15% damping with the modal frequency unchanged. (3) In case DV1, the modal frequencies of the uncontrolled modes do not shift significantly, while their damping ratios are increased considerably. This implies that the control spillover does occur. However, the spillover does not destabilize the system but rather enhances the structural damping.

In Table 1, the three mode shapes in case DV123 and the first mode shape in case DV1 were determined by the procedure of "Best Achievable Eigenvector" described in the preceding section. The mode shapes resulting from the two control cases are complex vectors, whose elements are represented by the magnitudes and phase angles (in parentheses) in Table 1. These complex mode shapes were extracted from the lower-half portion of their corresponding eigenvectors (see Eq. 6) and were normalized with respect to the value of the first floor. Note that in the determination of the best achievable eigenvectors, the number of controllable elements in each eigenvector was taken as one, since from a two-dimensional view there was only one actuator placed in the first story of the model (so, $r = 1$).

5.3 Time domain data

The roof displacements of the building model subjected to the 1940 El Centro earthquake with PGA scaled down to 0.1 g are depicted in Figs. 5(a) and 5(b). The response of the uncontrolled model is also plotted (the dotted line) in both figures for comparison. From these figures, it is observed that both control cases are equally effective for suppressing the seismic motion of the structure, although control case DV1 used only the first floor response as the feedback signal. The roof response of the model excited by the Kobe earthquake was also tested and the results are depicted in Figs. 6(a) and 6(b). In these two figures, the responses for the two control cases are also very similar; therefore, the observation made in the El Centro earthquake is also true for the Kobe earthquake.

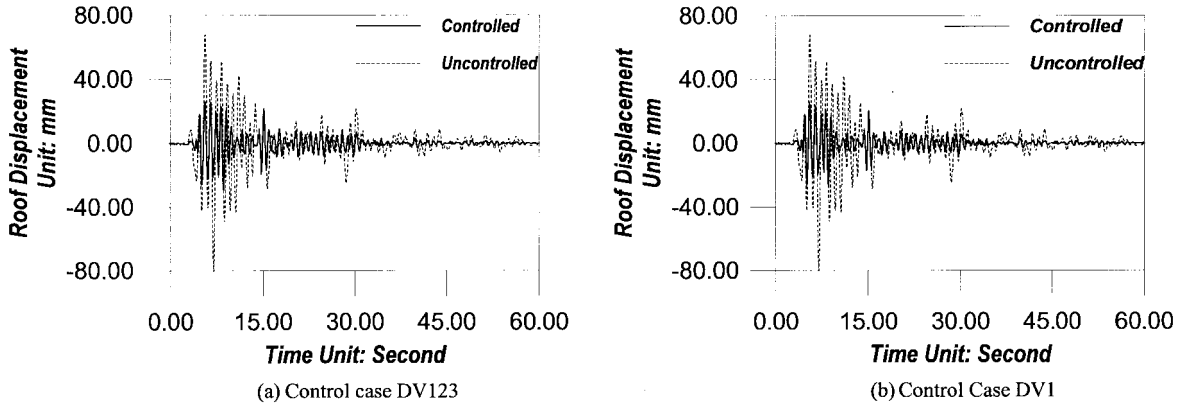

Fig. 5 Roof displacement of the steel frame subjected to El Centro earthquake

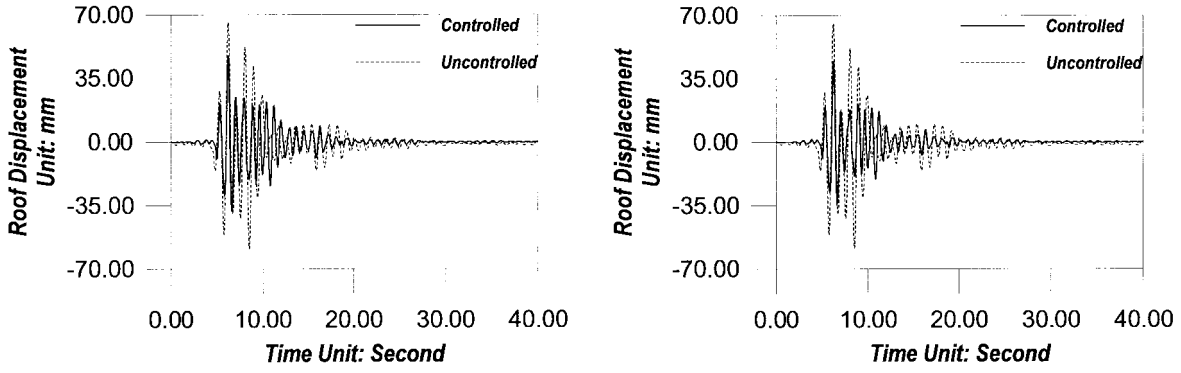

(a) Control case DV123 (b) Control Case DV1

Fig. 6 Roof displacement of the steel frame subjected to Kobe earthquake

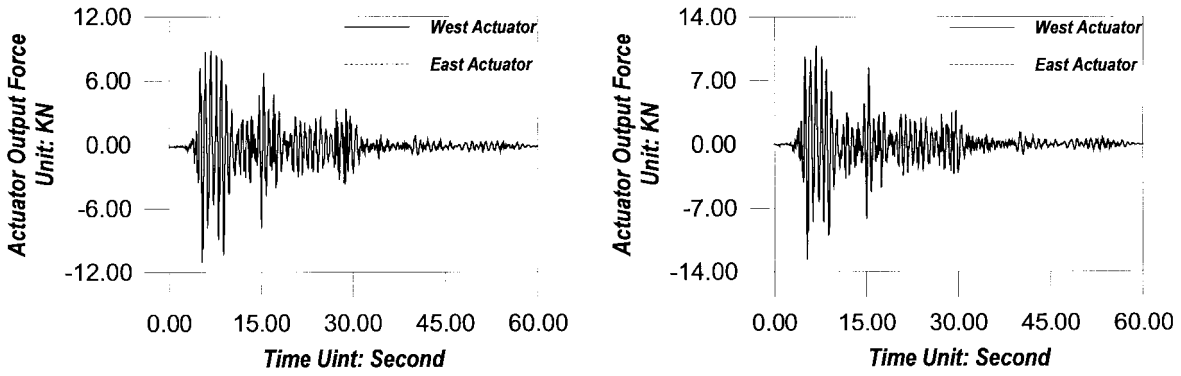

(a) Control Case DV123 (b) Control Case DV1

Fig. 7 Control force supplied by actuators for the steel frame subjected to El Centro earthquake

As for the concerns of control effort, Figs. 7(a) and 7(b) show the demand of control forces when the model is subjected to the El Centro earthquake. In the legend of the figures, the terms “East Actuator” and “West Actuator” are used to distinguish the two active braces installed on the two sides of the first floor. From these two figures, it is shown that both control cases require roughly equal control effort. Furthermore, in order to compare the control results at different floor levels, Fig. 8 plots the maximum floor displacement at each floor level for both control cases, when the model is excited by the El Centro earthquake. It can be seen that the reduction on the floor displacement is quite uniform along the story height for both control cases.

Tables 4 and 5 summarize the maximum values of the roof displacement, the displacement reduction rates and the control forces for different earthquakes. The reduction rate is obtained by dividing the difference of the maximum uncontrolled and controlled displacements by the uncontrolled values. Numerical simulation results, that used the structural matrices listed in Table 2, are also included in the tables to check the reliability of the test data. The deviation between the analytical and experimental results in Tables 4 and 5 may be contributed by the error of system identification. From Tables 4 and 5, it can be observed that: (1) In spite of the different nature of the El Centro and Kobe earthquakes, the direct output control (cases DV1) has a roughly equal

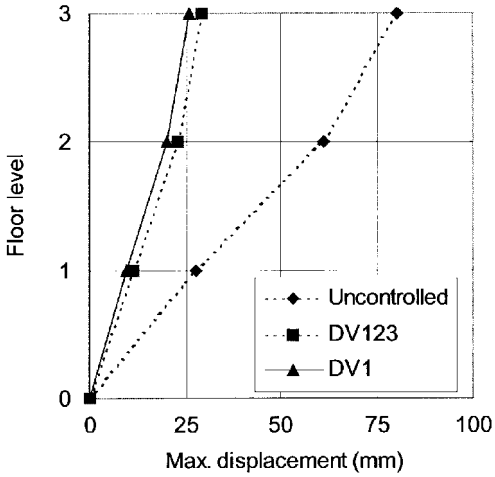

Fig. 8 Comparison of the maximum floor displacements for the steel frame subjected to El Centro Earthquake

Table 4 Comparison of maximum roof displacement and control force of the structure subjected to El Centro earthquake

Control case	Analytical value		Experimental values		
	Max. control force (kN)	Max. disp. (mm)	Max. control force (kN)	Max. disp. (mm)	Disp. reduction rate (%)
Uncontrolled	–	–	–	80.21	–
DV123	9.62	21.52	10.99	29.02	63.82
DV1	9.12	22.75	12.61	25.85	67.77

Table 5 Comparison of maximum roof displacement and control force of the structure subjected to Kobe earthquake

Control case	Analytical value		Experimental values		
	Max. control force (kN)	Max. disp. (mm)	Max. control force (kN)	Max. disp. (mm)	Disp. reduction rate (%)
Uncontrolled	–	–	–	65.71	–
DV123	13.70	39.12	12.20	47.27	28.06
DV1	13.18	40.13	13.65	44.54	32.22

reduction rate to that of full-state feedback control (case DV123) for both earthquakes. (2) Although control case DV1 requires slightly larger control forces for both earthquakes, it gives larger vibration reduction rates than those of case DV123. (3) The reduction rates of the El Centro earthquake for both control cases exceed 60% and are much better than those of the Kobe earthquake, in which only about 30% reduction rates were achieved. This implies that the performance of the control still depends on the nature of the ground excitation. The deterioration of the control performance may be caused by the coincidence of the main structural frequency with the pre-dominant frequency of the earthquake.

6. Influence of sensor noise and modeling error

In practice, an implemented active structural control system may suffer from sensor noise and modeling error; therefore, the control algorithm must be robust to these errors that may not be considered in the control design phase. In the test described previously, these two practical concerns did not cause problem or deterioration to the control system. However, in order to investigate how the proposed control method performs in the presence of sensor noise or modeling error, in this section, the influence of sensor noise or modeling error on the controlled structural response is studied numerically. Various levels of error and noise were simulated and introduced to the control case DV1. In the simulation, the structural mass, stiffness and damping matrices shown in Table 2 were employed and the El Centro earthquake record with its original PGA (0.34 g) was used as the ground excitation.

6.1 Influence of sensor noise

In the presence of signal noise, the output vector $\mathbf{y}(t)$ that contains sensor measurements can be rewritten as

$$\hat{\boldsymbol{y}}(t) = \boldsymbol{y}(t) + \boldsymbol{y}_n(t) = \boldsymbol{C}\boldsymbol{x}(t) + \boldsymbol{y}_n(t) \tag{30}$$

where $\hat{\boldsymbol{y}}(t)$ and $\boldsymbol{y}_n(t)$ denote the contaminated output vector and the noise vector, respectively. Sensor noise is usually caused by electrical noise that is normally in a form of broad-band signal and can be simulated by Gaussian white noise, i.e., white noise with Gaussian stochastic process (Bendat and Piersol 1991). A sample function of Gaussian white noise may be simulated by the following equation (Clough and Penzien 1993)

$$y_{n,i}(t) = 2\sqrt{\Delta\omega}\sqrt{S_{nn,i}}\sum_{k=1}^{N}\cos(k\cdot\Delta\omega\cdot t + \alpha_k) \tag{31}$$

where $y_{n,i}(t)$ denotes the noise of the i-th sensor measurement (i.e., the i-th element of $\boldsymbol{y}_n(t)$); $\Delta\omega$ is the sampling frequency; N is the number of the sampling frequencies; $S_{nn,i}$ is the power spectral density of the noise associated with the i-th measurement; α_k is a random variable uniformly distributed between 0 and 2π. Note that $S_{nn,i}$ is a constant for a white noise signal. Also, in order to quantify the level of the noise, let us define a noise ratio γ

$$\gamma = \frac{S_{nn,i}}{\bar{S}_{yy,i}} \tag{32}$$

where $\bar{S}_{yy,i}$ is the average power spectral density of the i-th measurement of the structural response over a given frequency range. Recall that in the control case DV1, one velocity and one displacement sensors were installed at the first floor of the three-story model. In order to generate noise records associated with these two sensor measurements, the following numerical values for the parameters appearing in Eqs. (31) and (32) were used in the simulation: $\Delta\omega = 0.02$ Hz; $N = 1500$ (equivalent to a frequency bandwidth ω_n of 30 Hz); α_k was randomly generated by a computer subroutine; $\bar{S}_{yy,v} = 8.93\times10^{-3}$ $((\mathrm{m/s})^2/\mathrm{Hz})$; $\bar{S}_{yy,d} = 1.86\times10^{-4}$ $(\mathrm{m}^2/\mathrm{Hz})$, (where $\bar{S}_{yy,v}$ and $\bar{S}_{yy,d}$ denote the average spectral densities of the velocity and displacement measurements, respectively). Note that in determining the values of $\bar{S}_{yy,v}$ and $\bar{S}_{yy,d}$, the spectral density functions

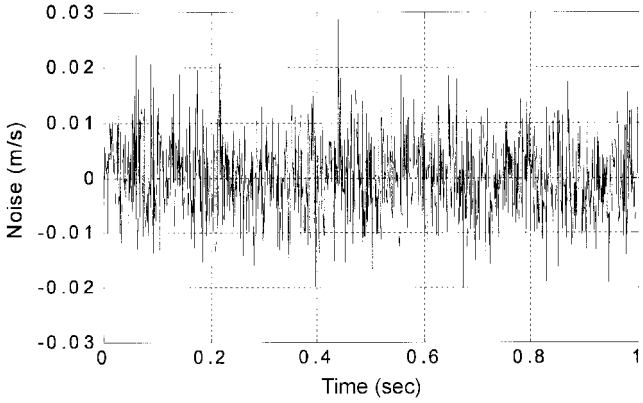

Fig. 9 A sample function of measurement noise for velocity sensor installed at the first floor (with noise ratio $\gamma = 0.01$)

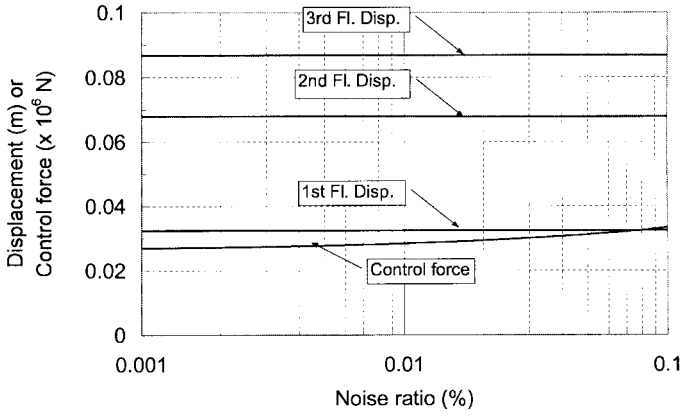

Fig. 10 Effect of sensor noise on the maximum floor displacements and control force

were calculated based on the first 50-second time-history data of the first-floor response (when the structure was controlled by the case DV1); afterward, the averages of the spectral density functions within 0-10 Hz were taken in the computation of $\bar{S}_{yy,v}$ and $\bar{S}_{yy,d}$ (the spectral density functions approach zero for frequencies above 10 Hz). Fig. 9 shows the simulated noise record for the velocity measurement with a noise ratio γ of 0.01.

Considering the control case DV1 and assuming the displacement and velocity sensors have the same noise ratio, Fig. 10 shows the effect of the noise ratio γ on the maximum relative floor displacements and the maximum control force. Note that a sensor signal with γ greater than 0.01 can be considered as a heavily contaminated signal, because when the noise ratio γ, which is a spectral ratio, is equal to 0.01, the root mean square (RMS) ratio of the noise to signal is of the order of 10%. Figs. 11(a) and 11(b) show the time histories of the control forces without and with the presence of the sensor noise (with $\gamma = 0.01$), respectively. For $\gamma = 0.01$ and 0.1, the numerical values of the maximum structural responses are also summarized in Table 6. From Fig. 10, Fig. 11 and Table 6, it is observed that: (1) Due to the presence of the sensor noise, the time history of the control force contains high-frequency components (see Fig. 11b). The peak values of the control

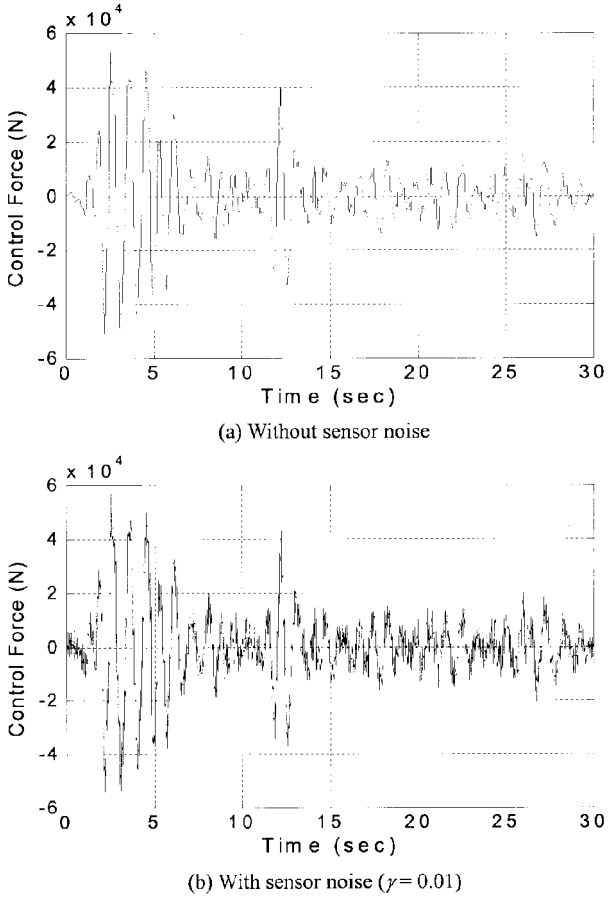

Fig. 11 Comparison of control forces without and with sensor noise

Table 6 Comparison of maximum control force and roof response in the presence of modeling error or sensor noise

Control condition	Magnitude of error or noise	Control force[1] (kN)	Max. response of roof	
			Acceleration[1] (m/s^2)	Relative displ.[1] (m)
DV1	Non	52.9 (1.00)	5.87 (1.00)	0.0868 (1.00)
DV1 w/ sensor noise	γ = 0.01	56.7 (1.07)	5.87 (1.00)	0.0868 (1.00)
	γ = 0.1	66.5 (1.27)	5.88 (1.00)	0.0867 (1.00)
DV1 w/ modeling error	ε_k = 10%	57.2 (1.08)	6.41 (1.09)	0.0859 (0.99)
	ε_k = 25%	61.4 (1.16)	7.26 (1.24)	0.0821 (0.95)

[1] Value in parentheses denotes the ratio to that of the case without noise or error.

force are increased by 7.2% and 25.7%, for γ = 0.01 and 0.1, respectively. (2) Although the control force is considerably affected by the sensor noise, the structure is still stable and the noise does not have much influence on the floor displacements even with a noise ratio γ as high as 0.1 (see Fig.

10). The reason for the second observation is explained below. Because a high-frequency excitation may not cause much influence on a structure with a low natural frequency, the high-frequency components of the control force, which is due to the sensor noise, has very little effect on the dynamic response of the model structure that has all modal frequencies lower than 6 Hz (see Table 1). Nevertheless, the increase on the control force surely introduces extra internal forces in the structural members, especially the columns; therefore, a large sensor noise should be avoided, even though it may not destabilize the modal controlled structure.

6.2 Effect of modeling error

Modeling errors can be caused by inaccurately estimating any of the three structural matrices, namely, the mass, damping and stiffness matrices, see Eq. (1). The inaccuracy may further cause an error on the estimation of the modal parameters, which are required in the computation of the feedback gain for the proposed model control method, and finally results in deterioration of the control performance. Among the three structural matrices, the damping matrix is usually a postulated one and is normally assumed to be a function of mass and stiffness matrices if the proportional damping is adopted. The damping matrix may have relatively small values for a lightly damped structure, which is the case for most of building structures. On the other hand, the mass matrix can be more precisely computed from the densities of the constitutive materials of the structure. The stiffness matrix is the one that has the highest possibility of introducing a large modeling error, for it is difficult to accurately model some of structural behaviors, such as stiffness of shear walls or partition wall, combination stiffness of slab and girders, the semi-rigidity behavior of member joints, etc. Since the stiffness matrix is most likely to introduce a large modeling error, in this study, only the effect of the stiffness error on the control performance was investigated.

For the convenience of discussion, let us assume that the relation of the actual stiffness $\hat{\boldsymbol{K}}_s$ and the estimated stiffness $\boldsymbol{K}_s$ has the following form

$$\hat{\boldsymbol{K}}_s = \boldsymbol{K}_s + \Delta\boldsymbol{K}_s = (1 + \varepsilon_k)\boldsymbol{K}_s \tag{33}$$

where $\Delta\boldsymbol{K}_s$ and ε_k denote the error stiffness matrix and the ratio of the error matrix, respectively. The variable ε_k that can be a negative or positive real number represents a measurement of the error magnitude. After $\boldsymbol{K}_s$ is replaced by $\hat{\boldsymbol{K}}_s$ in Eq. (4), the system matrix $\boldsymbol{A}$ becomes a function of ε_k and may be denoted by $\hat{\boldsymbol{A}}(\varepsilon_k)$. Accordingly, Eq. (9) must be modified as

$$\dot{\boldsymbol{x}} = (\hat{\boldsymbol{A}}(\varepsilon_k) + \boldsymbol{BFC})\boldsymbol{x} + \boldsymbol{f}\,\ddot{x}_g = \hat{\boldsymbol{A}}_c(\varepsilon_k)\boldsymbol{x} + \boldsymbol{f}\,\ddot{x}_g \tag{34}$$

where $\hat{\boldsymbol{A}}_c(\varepsilon_k)$ denotes the closed-loop system matrix with modeling error ε_k. In the last equation the feedback gain $\boldsymbol{F}$ is designed based on $\boldsymbol{A}_c$ with the estimated stiffness $\boldsymbol{K}_s$, not on $\hat{\boldsymbol{A}}_c(\varepsilon_k)$. Eq. (34) was used for simulating the response of the controlled structure with modeling error and the result is shown below. Note that in Eq. (34) the control stability of the closed-loop system can be determined by the signs of the real parts of the $\hat{\boldsymbol{A}}_c(\varepsilon_k)$ eigenvalues, or by the signs of the equivalent damping ratios ζ_i ($i = 1\sim n$) computed by Eq. (7), as discussed previously. The modal control becomes unstable if at least one of the closed-loop modes has the negative ζ_i.

Figs. 12(a) and 12(b) show all modal frequencies and damping ratios of the controlled structure as functions of the modeling error ε_k. From these two figures it is shown that: (1) For a modeling

error $|\varepsilon_k|$ up to 25%, the control system is still stable, since all damping ratios remain positive, see Fig. 12(b). There remains a large control stability margin for $|\varepsilon_k| > 25\%$. (2) When the structural stiffness is underestimated ($\varepsilon_k > 0$) during the design of feedback gain, the resulting modal frequencies of the controlled structure become larger than the expected ones (the dashed lines in Fig. 12), and in contrast the resulting damping ratios are lower than the expected values. This implies that the proposed model control method with an underestimated structural stiffness produces a stiffer but less damped structural system. The situation for the closed-loop modal parameters will be reversed if the structural stiffness is overestimated ($\varepsilon_k < 0$). Fig. 13 shows the effect of ε_k on the maximum relative floor displacements and maximum control force, when the structure is excited by the El Centro earthquake. From Fig. 13, it is observed that: (1) For a modeling error $|\varepsilon_k|$ up to 25%, the influence on the floor displacements is marginal and on the control force is not very significant, either. (2) When the structural stiffness is underestimated ($\varepsilon_k > 0$), the applied control force is increased, and at the meantime the floor displacements are decreased. This implies that the extra control effort does not destabilize the control system, but rather it suppresses the motion of the structural displacements. In Table 6, it is shown that when $\varepsilon_k = +25\%$, the absolute acceleration of the top floor is increased by 24%, although the floor displacement is reduced by 5%. This implies

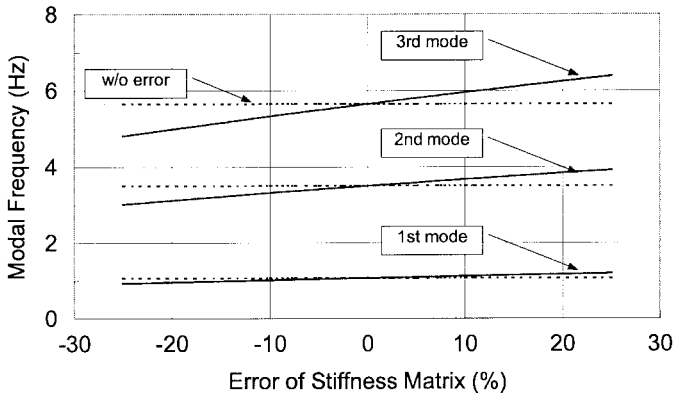

(a) Modal frequencies

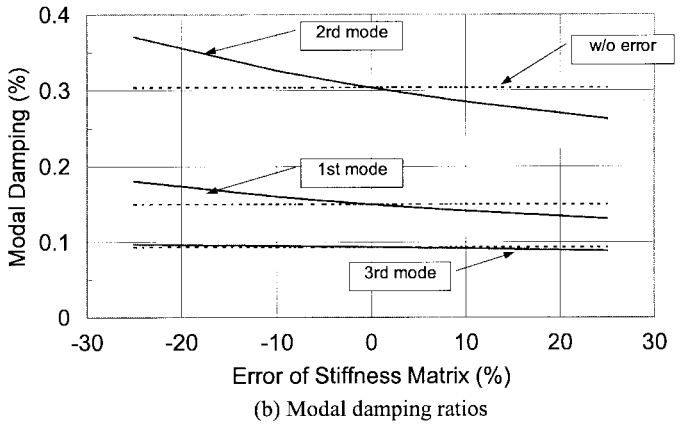

(b) Modal damping ratios

Fig. 12 Effect of stiffness error on the modal properties of the controlled structure (dash lines represent modal values without error)

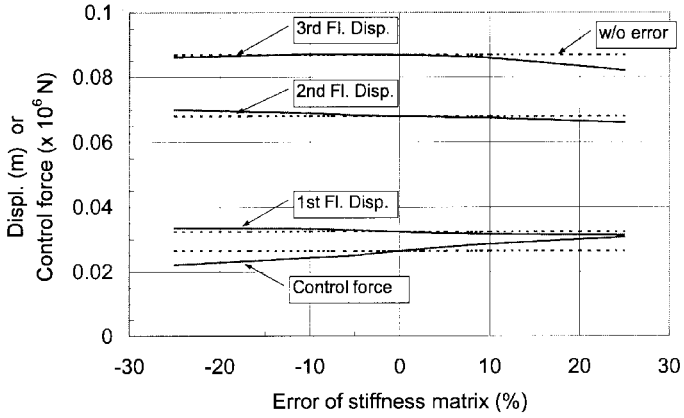

Fig. 13 Effect of Stiffness error on the maximum floor displacements and control force (dash lines represent responses without error)

that the stiffness modeling error is more critical to the structural accelerations than to the displacements for the proposed model control. This unexpected increase of the acceleration may not destabilize the control system but may greatly deteriorate the control performance and thus it should be carefully dealt with if a stiffness error may exist.

7. Conclusions

In this paper, the computation of the feedback gain for modal control with direct output feedback is formulated in a concise matrix form. With this gain matrix, the number of the controllable eigenvalues is equal to the number of the sensors installed on the structure, while the number of the actuators available decides the number of the controllable elements in each controlled eigenvector. A method for generating the best achievable eigenvectors that are most consistent with the desired ones is also proposed. For experimental verification, the proposed control method was applied to a full-scale building model for suppressing its seismic motion. The model, which was equipped with an active bracing system, was placed on an earthquake simulation table for the test. For comparison, two modal control cases, one with full-state feedback and the other with direct output feedback, were tested and the experimental result is presented. The latter control case requires very few sensors for feedback control. It is shown by the test results that although the latter control case requires slightly higher control effort than the former one, the two control cases are equally effective in mitigating the seismic response of the building model. Finally, the control performance of the proposed method in the presence of sensor noise and modeling error is also investigated. The numerical result shows that although the maximum control force may be increased, the maximum structural displacements are very insensitive to sensor noise and modeling error, when Gaussian white noise and structural stiffness error are considered. This implies that sensor noise and modeling error may be influential to the control performance, but they do not easily cause control stability problem.

Acknowledgments

This research was sponsored in part by the National Center for Research on Earthquake Engineering (NCREE) and also by National Science Council, Taipei, Taiwan. The author is grateful to Dr. L. L. Chung and Mr. S. K. Huang at NCREE for their assistance with the experimental work, and also to his graduate student Mr. G. L. Lin at National Kaohsiung First University of Science & Technology for preparing some of the simulation data.

References

Andry, A.N., Shapiro, E.Y., and Chung, J.C. (1983), "Eigenvalue assignment for linear systems", *IEEE Transaction on Aerospace and Electronic Systems*, **19**(5), 711-728.

Balas, M.J. (1979), "Direct output feedback control of large space structures", *J. Astronaut. Sci.*, **27**(2), 157-180.

Baruh, H. (1987), "A recursive pole placement method for large flexible structures", *Proc. of ASME Design Technology Conference, 11th Biennial Conference on Mechanical Vibration and Noise*, 79-84.

Bendat, J.S., and Piersol, A.G. (1991), *Random Data*, 2nd edn., John Wiley & Sons Inc., Singapore.

Chang, C.-C., and Yu, L.-O. (1998), "A simple optimal pole location technique for structural control", *Eng. Struct.*, **20**(9), 792-804.

Chang, M.I.I. and Soong, T.T. (1980), "Optimal controller placement in modal control of complex system", *J. Math. Anal. and Appl.*, **75**, 340-358.

Clough, R.W., and Penzien, J. (1993), *Structural Dynamics*, 2nd edn., McGraw Hill Inc., 492-498.

Davison, E.J. (1970), "On pole assignment in linear system with incomplete state feedback", *IEEE Transactions on Automatic Control*, **15**, 348-351.

Davison, E.J., and Wang, S.H. (1975), "On pole assignment in linear multivariable systems using output feedback", *IEEE Transactions on Automatic Control*, **20**, 516-518.

Dyke, S.J., Spencer, B.F., Quast, P., Sain, M.K., Kaspari, D.C., and Soong, T.T. (1996a), "Acceleration feedback control of MDOF structures", *J. Eng. Mech.*, ASCE, **122**(9), 907-918.

Dyke, S.J., Spencer, B.F., Quast, P., Kaspari, D.C., and Sain, M.K. (1996b), "Implementation of an active mass driver using acceleration feedback control", *Microcomputers in Civil Engineering: Special Issue on Active and Hybrid Structural Control*, **11**, 305-323.

Kautsky, J., and Nichols, N.K. (1985), "Robust pole assignment in linear state feedback", *Int. J. Control*, **41**(5), 1129-1155.

Kimura, H. (1975), "Pole assignment by gain output feedback", *IEEE Transactions on Automatic Control*, **20**, 509-516.

Kurata, N., Kobori, T., Motoichi, T., Niwa, N., and Midorikawa, H. (1999), "Actual seismic response controlled building with semi-active damper system", *Earthq. Eng. and Struct. Dyn.*, **28**(11), 1427-1447.

Lu, L.Y., Bain, J.J., and Chung, L.L. (1999), "Use of the active member concept in vibration mitigation of seismic structures", *Eng. Struct.*, **21**(4), 341-351.

Lu, L.Y., Utku, S., and Wada, B.K. (1993), "Vibration suppression for large scale adaptive truss structures using direct output feedback control", *J. of Intelligent Mater. Sys. and Struct.*, **4**(3), 385-397.

Maghami, P.G., and Juang, J.N. (1989), "Efficient eigenvalue assignment for large space structures", *Proc. of AIAA/ASME/ASCE/AHS 30th Structures, Structural Dynamics, and Materials Conference*, Mobil, AL, USA, 2037-2045.

Meirovitch, L. (1990), *Dynamic and Control of Structures*, John Wiley & Sons, New York, USA.

Moore, B.C. (1976), "On the flexibility offered by state feedback in multivariable systems beyond closed loop eigenvalue assignment", *IEEE Transaction on Automatic Control*, **21**, 689-692.

Nishitani, A. (1998), "Application of active structural control in Japan", *Progress in Structural Engineering and Materials*, **1**(3), 301-307.

Öz, H., and Meirovitch, L. (1980), "Optimal modal-space control of flexible gyroscopic systems", *J. Guidance*

and Control, **3**(3), 218-226.
Porter, B., and D'Azzo, J.J. (1978), "Closed loop eigenstructure assignment by state feedback in multivariable linear system", *Int. J. of Control*, **27**(3), 487-492.
Simon, J.D., and Mitter, S.K. (1968), "A theory of modal control", *Information and Control*, **3**, 316-353.
Soong, T.T. (1990), *Active Structural Control - Theory and Practice*, Longman, London (U.K.).
Srinathkumar, S. (1978), "Eigenvalue/eigenvector assignment using direct output feedback", *IEEE Transaction on Automatic Control*, **23**(1), 79-81.
Varga, A. (1981), "A Schur method for pole assignment", *IEEE Transactions on Automatic Control*, **26**(2), 517-519.
Wonham, W.M. (1967), "On pole assignment in multi-input, controllable linear systems", *IEEE Transaction on Automatic Control*, **12**, 660-665.